Int. J. Heat Mass Transfer. Vol. 36, No. 11, pp. 2815–2826, 1993
Printed in Great Britain

0017–9310/93 $6.00+0.00

Modeling of turbulent buoyant flow and heat transfer in liquid metals

A. A. MOHAMAD and R. VISKANTA
School of Mechanical Engineering, Purdue University, West Lafayette, IN 47907, U.S.A.

(*Received* 1 *May* 1992 *and in final form* 25 *November* 1992)

Abstract—Turbulent natural convection in a cavity filled with low Prandtl number fluids is investigated. The cavity is either heated from below and cooled from above or heated differentially and the other connecting walls are assumed to be thermally insulated. Direct numerical simulations, and two- and three-dimensional low Reynolds number k–ε turbulence models are used. It is shown that the turbulent Prandtl number equal to one or slightly greater than one produces useful results, regardless of the value of molecular Prandtl number. A correlation is suggested for the Nusselt number as a function of $Ra\,Pr$ (Boussinesq number) for natural convection in a differentially heated cavity. The flow becomes turbulent for $Ra\,Pr > 4.8 \times 10^3$.

INTRODUCTION

NATURAL convection of liquid metals has been a subject of study by nuclear reactor engineers and metallurgists. Liquid metals are excellent heat transfer media. During shut down of a liquid metal cooled nuclear reactor, heat transfer from the reactor core to the liquid metal coolant takes place by natural convection. In severe nuclear reactor accidents heat transfer in the molten core debris takes place by buoyancy driven convection. Natural convection in low Prandtl number fluids has undesirable effects in crystal growth in the Bridgman bath or Chochrawlski apparatus, because the migration of the impurities by natural convection affects the quality of the crystal. Also, oscillation of temperature due to instability of the buoyant flow of liquid metals induces nonuniform cooling at the solidification front. In casting and material processing it is very important to keep the melt at a uniform temperature during the solidification in order to decrease the thermal stresses. Hence, understanding of the flow and heat transfer in liquid metals is essential in many processes including those mentioned above. Since the kinematic viscosity of a liquid metal is very small and the liquid metal containers can be large, the flow is characterized as turbulent. Hence, it is very difficult to maintain laminar flow conditions in practical systems.

Experimentation with liquid metals is difficult, and very few experiments with buoyancy driven flow have been performed. Transport phenomena in liquid metal flows are not as fully understood in comparison with the flow and heat transfer in ordinary liquids such as air and water. Experimental natural convection heat transfer data have been correlated as functions of the Grashof or Rayleigh numbers. The data are limited to laminar flow, and very few data are available for the turbulent flow regime [1–5].

Natural convection in a differentially heated cavity has been studied [6–9]. Results showed that the buoyant flow in a differentially heated cavity can differ in essential ways from the flow of ordinary liquids [8, 9]. Thermal diffusion in a liquid metal is important, and the hydrodynamic boundary layer is very thick for buoyancy driven flows; while for ordinary fluids the hydrodynamic boundary layers are thin, and the maximum velocity of ascending and descending flow occurs near the boundaries. Another feature of the buoyant flow in a liquid metal is the formation of weak secondary circulations in the corners of the cavity. Flow separation takes place at the corners, because the peaks of ascending and descending velocities occur far away from the boundaries, leading to formation of secondary circulations in these regions. Also, the core of the cavity may contain several secondary circulations rotating inside the main circulation. As discussed elsewhere [8, 10], the first evolution process of such weak secondary circulation is in the upper right-hand corner (near the cold wall) of the cavity and by skew symmetry in the lower left-hand corner (near the hot wall). The reason that these corners are more unstable than the remaining ones is that the hot (low density) fluid is below the cold (high density) fluid, which produces unstable flows in these corners.

The process of transition to turbulent flow is discussed by Mohamad and Viskanta [10]. The turbulent buoyant flow of low Prandtl number fluids has not been addressed and is the subject of the present work. Currently, the attention of a turbulent modeler has been focused on the low Reynolds number (LRN) k–ε turbulence model and the Reynolds stress transport term-by-term modeling, and to some extent on large scale and direct numerical modeling [11]. The latter modeling process requires extensive computer resources and presently is not practical for more routine engineering design calculations. The term-by-term Reynolds stress approach requires tuning of the empirical model constants and requires greater computer time resources compared to the k–ε turbulence

NOMENCLATURE

A aspect ratio, H/L
Bo Boussinesq number, $Ra\,Pr$
f dimensionless frequency, $(1/\tau)$
Gr Grashof number, $\beta g H^3 \Delta T/\nu^2$
H height of the cavity [m]
h convective heat transfer coefficient [W m^{-2} K]
k thermal conductivity [W m^{-1} K^{-1}]
L length of the cavity [m]
Nu Nusselt number, hH/k
Nu_{av} spatially averaged Nusselt number, $-\int_0^1 (\partial\theta/\partial\xi)|_{\xi=0,1}\,d\eta$
p pressure [Pa]
Pe Peclet number, $Re\,Pr$
Pr molecular Prandtl number, ν/α
Pr_t turbulent Prandtl number, $\varepsilon_m/\varepsilon_h$
Ra Rayleigh number, $Gr\,Pr$
Re Reynolds number
t time [s]
T temperature [K]
T_h, T_c hot and cold wall temperatures [K]
u, v, w velocity components in the x-, y- and z-directions, respectively [m s^{-1}]
U, V, W dimensionless velocity components in ξ-, η- and ζ-directions.

Greek symbols
α thermal diffusion coefficient [m^2 s^{-1}]
ΔT temperature difference, $(T_h - T_c)$ [K]
ε_h eddy diffusivity of heat [m^2 s^{-1}]
ε_m eddy diffusivity of momentum [m^2 s^{-1}]
ζ dimensionless z-coordinate, z/H
η dimensionless y-coordinate, y/H
θ dimensionless temperature, $(T-T_c)/(T_h-T_c)$
μ molecular viscosity [kg m^{-1} s^{-1}]
μ_t turbulent viscosity [kg m^{-1} s^{-1}]
ν kinematic viscosity [m^2 s^{-1}]
ξ dimensionless x-coordinate, x/H
ρ density [kg m^{-3}]
τ dimensionless time, $(\alpha t/H^2)$.

Superscripts
time averaged quantities
fluctuating component.

model. For natural convection the Reynolds stress term-by-term modeling (algebraic stress model) does not produce significantly improved results over the LRN k–ε turbulence model in average velocities, temperature and rate of heat transfer predictions [12].

The difference between liquid metal and ordinary fluids is the Prandtl number. Liquid metals in general have higher thermal diffusivity and lower kinematic viscosity compared with ordinary fluids. Hence, it is assumed that the only difference between turbulent modeling using eddy diffusivity approach (LRN k–ε) for liquid metals is correctly evaluating the turbulent Prandtl number. There is some evidence that the turbulent Prandtl number should be greater than unity, which is usually the value reported for ordinary fluids. In this work a review is presented of different models which have been suggested for correlating turbulent Prandtl number. Then, different flow conditions are examined for which the available experimental data and numerical results of two- and three-dimensional models are evaluated on the bases of experimental data and direct numerical simulation results.

TURBULENT PRANDTL NUMBER

The turbulent Prandtl number is the ratio of the eddy diffusivity of momentum to the eddy diffusivity of the enthalpy (heat) and is defined as

$$Pr_t = \varepsilon_m/\varepsilon_h \tag{1}$$

which is analogous to the definition of molecular Prandtl number ($Pr = \nu/\alpha$). The turbulent Prandtl number is a function of the Reynolds number, Prandtl number, and flow conditions [13]. However, useful results can be obtained by assuming that Pr_t is uniform across the flow region [12, 14, 15]. A simple analysis based on the gradient diffusion model of the diffusivity can yield an expression for turbulent Prandtl number [14]

$$Pr_t = \frac{1+86Pe^{-1/2}}{1+200Re^{-1/2}}. \tag{2}$$

Other expressions have been reviewed by Reynolds [16]. For ordinary fluids ($Pr \geqslant 1$) a constant value of the order one ($Pr_t = 0.9$–1.0) was used to successfully predict the shear and buoyant flows [12, 15].

Buhr *et al.* [17] studied mixed convection flow of mercury in a vertical pipe and concluded that the eddy diffusivity ratio is greater than one. Azer and Chao [18] suggested a formula based on the experimental work on the flow of a liquid metal through a pipe. Lykoudis and Touloukian [19] derived an expression for turbulent Prandtl number as a function of the molecular Prandtl number

$$Pr_t^{-1} = \frac{6}{\pi^2}[e^{-0.01/Pr} + \tfrac{1}{4}e^{-0.04/Pr} + \cdots]. \tag{3}$$

Also, Deissler [20] suggested a formula for Pr_t as a function of Pr only

$$Pr_t = \left\{\left[2.05Pr\left(1-\frac{Pr}{1+Pr}\right)^{1.5}\right]\Big/(1-Pr)\right\}^{-1}. \tag{4}$$

Cotton *et al.* [21] tested three formulas suggested by Reynolds [16]

$$Pr_t = 1 + 100 Pe^{-1/2} \left(\frac{1}{1 + 120 Re^{-1/2}} - 0.15 \right)^{-1}. \quad (5)$$

Aoki [22]

$$Pr_t^{-1} = 0.014 Re^{0.45} Pr^{0.2} \left(1 - \exp\left(- \frac{1}{0.014 Re^{0.45} Pr^{0.2}} \right) \right) \quad (6)$$

and Jischa and Rieke [23]

$$Pr_t = 0.9 + \frac{182.4}{Pr\, Re^{0.888}}. \quad (7)$$

The tests were for mixed flow in a vertical pipe and for $Pr < 1$ using the low Reynolds number k–ε turbulence model. The predicted Nusselt numbers showed little difference.

The Soviet literature has indicated that the turbulent Prandtl number for liquid metals is slightly greater than unity [24, 25]. Potemkin [26] stated that the turbulent Prandtl number is a weak function of the molecular Prandtl number for $Pr \leqslant 1$. Similarly, Golubev [27] used $Pr_t = 1$ for convective flow of a liquid metal with $Pr = 0.0053$.

A significant research effort has been, and continues to be, devoted to the evaluation of the turbulent Prandtl number for liquid metals [28, 29]. These efforts are based either on experimental work or on the scale analysis arguments. The major conclusions are that for forced flow the turbulent Prandtl number approaches unity as the Reynolds number increases. The turbulent Prandtl number increases as the molecular Prandtl number decreases. Also, the turbulent Prandtl number increases near the boundaries. All these conclusions are for forced flow, and there have been no tests for buoyant or mixed flow to show if the predictions of the models are consistent with the experimental data using different approaches by including in the model both molecular and turbulent Prandtl numbers. Finally, most authors have used their correlations to show agreement with the experimental data, without further considering the comparison with results based on turbulent Prandtl number of unity or based on simple models.

ANALYSIS

Mathematical model

The geometry under consideration is a rectangular box, with y-axis in the vertical direction parallel to the gravitational field, and x- and z-axes form a horizontal plane. A cavity filled with low Prandtl number fluids and either heated from below and cooled from above or heated from the left-hand side and cooled from the right-hand side. The connecting walls are assumed insulated thermally. The equations that govern the physics of the flow can be described by Navier–Stokes equations (continuity, momentum and energy). Assuming incompressible flow, constant thermophysical properties, except for variation of density with temperature in the buoyancy force (i.e. the Boussinesq approximation is valid), the governing equations can be written as [30]

continuity

$$\frac{\partial U_i}{\partial x_i} = 0 \quad (8)$$

momentum

$$\frac{\partial (U_i)}{\partial \tau} + \frac{\partial (U_j U_i)}{\partial x_j} = - \frac{\partial P}{\partial x_i} + Pr \frac{\partial}{\partial x_j} \left(\frac{\partial U_i}{\partial x_j} \right) + \delta_{2i}\, Bo\, \theta \quad (9)$$

energy

$$\frac{\partial \theta}{\partial \tau} + \frac{\partial}{\partial x_j} (U_j \theta) = \frac{\partial}{\partial x_j} \left(\frac{\partial \theta}{\partial x_j} \right). \quad (10)$$

Scales of H, H^2/α, α/H, and ΔT are used for length, time, velocity and temperature, respectively. In the direct numerical simulation the above equations are solved (i.e. three-dimensional unsteady). The low Reynolds number k–ε turbulence model used in this paper is described in detail by Mohamad and Viskanta [31] and need not be repeated.

For the solution of the above equations it is assumed that there is no slip at the boundaries, i.e. the velocity component is set to zero at the boundaries. Temperature gradient normal to the wall is set to zero at the adiabatic boundaries, and the temperature is specified for heated and cooled walls.

Method of solution

A control volume, finite-difference technique was used to solve the model equations with appropriate boundary conditions. The SIMPLER algorithm was employed to solve the equations in primitive variables [32].

The governing equations are converted to systems of algebraic equations through an appropriate integration over each control volume of the domain and finite-difference approximation of partial derivatives. The algebraic equations are solved using a line-by-line iterative method coupled with an additive correction procedure to speed the convergence. The method solves a line of nodes using the tridiagonal matrix inversion algorithm and sweeps the domain of the integration in different directions along the axes. Fully implicit Euler method was used to march the solution in time. Very large time steps were used when the interest focused on the final steady state solutions. When the interest was in the unsteady and transient solution, a second-order predictor–corrector scheme was used for the time-marching.

Second order central-difference discretization of the diffusive–advective flux is used for the spatial derivatives. Hence, the second-order accuracy is ensured in time and space. This minimizes the false diffusion.

Table 1. Summary of the simulated cases and number of nodes used

	Model	Pr	Ra	Number of nodes	Aspect ratio, cavity dimensions and comments
Cavity heated from below	2-D, k–ε	0.022	1×10^6–1×10^9	131×41, 151×51	$A=1/10$
	2-D, k–ε	0.022	2.2×10^7	121×61	$A=1/2$
	2-D, k–ε	0.022	2.46×10^4	131×31	$A=1/10$
	3-D, unsteady	0.022	2.46×10^4	$121\times31\times51$	$10\times1\times5$ ($\Delta\tau=0.001$)
	3-D, unsteady	0.022	2.2×10^5–2.2×10^6	$31\times31\times31$	$2\times1\times2$ ($\Delta\tau=0.005$)
	3-D, unsteady	0.022	2.2×10^7	$41\times41\times41$	$2\times1\times2$ ($\Delta\tau=0.001$)
Differentially heated cavity	2-D, k–ε	0.022	2.2×10^5–2.2×10^9	61×61, 101×101, 81×41–151×41	$A=1$ to $1/6$
	2-D, k–ε	0.005	5×10^3–5×10^7	61×61	$A=1$
	3-D, k–ε	0.022	2.2×10^7	$31\times31\times31$	$1\times1\times1$
	3-D, unsteady	0.022	2.2×10^7	$31\times31\times31$	$1\times1\times1$ ($\Delta\tau=0.005$)

However, such a scheme requires very fine meshes and small time steps. Therefore, when the high accuracy is desired this scheme is preferable over the upwind scheme [33].

Grid independent results are ensured for the two-dimensional model. For three-dimensional models, fine meshes are used, but no grid independence tests have been carried out due to computer resource availability. The number of nodes for each case are summarized in Table 1.

RESULTS AND DISCUSSION

Cavity heated from below

The flow in a cavity depends on the Rayleigh number, Prandtl number and geometrical constraints. The flow may become turbulent in a shallow cavity filled with a liquid metal just above the threshold value (i.e. $Ra = 1708$) as the experiments of Ahlers and Behringer [34] have indicated. The mean temperature of the fluid at the core of the cavity is equal to the arithmetic average temperature imposed at the boundaries, and a major temperature drop takes place within the horizontal boundaries. The thickness of the thermal boundary layers decreases with increasing Rayleigh number and increases with decreasing molecular Prandtl number. Experimental data on liquid metals are very limited due to the difficulty of measurements. Only the average Nusselt number [35, 36] or the temporal variation of the temperature [37] are available. Mohamad [38] in his experiments recorded temperature profiles for liquid gallium in a cavity having dimensions $25.4\times2.54\times12.7$ cm in length, height and width, respectively.

A comparison between the experimental data and based on a two-dimensional LRN k–ε turbulence model (with 131×31 nodes and $Pr_t = 1.2$) and the three-dimensional full numerical simulation model ($121\times31\times51$ nodes) predictions are shown in Fig. 1 for a cavity filled with gallium ($Pr = 0.022$) for which $Ra = 2.46\times10^4$. The two-dimensional numerical model predicts that heat conduction dominates the flow at the core of the cavity, while the experimental data suggest that advection contributes significantly to the flow. Hence, the discrepancy can be understood by the presence of turbulence in the flow and the fact that the two-dimensional model suppresses the turbulence [39]. Therefore, a three-dimensional numerical simulation was undertaken to support the argument. The results show that the three-dimensional model predictions agree better with the experimental data than the two-dimensional model predictions. It is interesting to note that the average Nusselt number for the 2-D LRN k–ε turbulence model and unsteady full 3-D numerical calculations are 1.699 and 1.697, respectively. Such agreement is evident in Fig. 1, where the temperature gradients at the boundaries are the same for both models.

Table 2 summarizes the average Nusselt numbers of the two-dimensional predictions and compares them with the available experimental data and correlation. The data of Rossby [36] and the predictions of the LRN k–ε turbulence model underestimate the Nusselt number compared with the data of Globe and Drop-

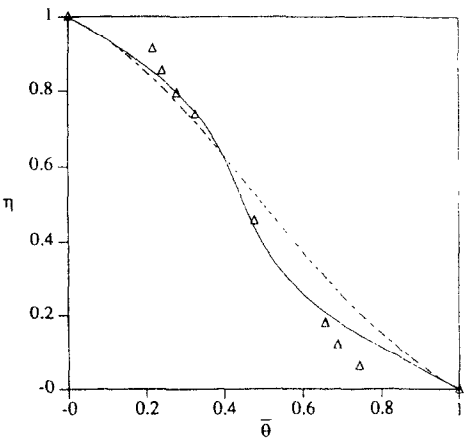

FIG. 1. Comparison of predictions of different models with experimental data for temperature profile in a cavity heated from below, $Ra = 2.464\times10^4$ and $Pr = 0.022$ (△, experiments [38]; ——, three-dimensional model prediction; — - - —, two-dimensional model prediction).

Table 2. Comparison of the 2-D k–ε turbulence model predictions of the average Nusselt number with available experimental data for $Pr = 0.022$

Ra	k–ε model	Globe and Dropkin [35]	Rossby [36] for $Pr = 0.025$
1×10^6	3.92	5.20	4.91–5.41
1×10^7	8.78	11.21	8.67–9.87
1×10^8	21.92	24.15	15.54–18.00
1×10^9	47.96	52.02	27.82–32.83

kin [35]; however, the results are within the experimental uncertainty of the data.

Direct numerical simulation was carried out for a cavity heated from below and filled with a liquid metal having Prandtl number of 0.022. (This value is typical of liquid gallium.) For mercury the value is 0.025. The dimension of the cavity was selected to be $2 \times 1 \times 2$ in ξ-, η- and ζ-directions, respectively. A nonuniform mesh of $31 \times 31 \times 31$ was adopted. The results for $Gr = 1 \times 10^7$ ($Ra = 2.2 \times 10^5$) showed that the flow is periodic with a dimensionless frequency of 12.68. Figure 2 shows the temporal variation of the V-velocity component at the center of the cavity and the corresponding spectral power. The flow becomes quasi-periodic as the Grashof number is increased to 1×10^8 as revealed in Fig. 3. This figure illustrates the temporal variation of the V-velocity component with the corresponding power spectra. Figure 4 shows the correlation $\overline{V'U'}$ and $\overline{V'\theta'}$ at the mid-plane of the cavity. The Reynolds stress $\overline{V'\theta'}$ has a maximum near the horizontal boundaries and drops to a minimum at the center of the cavity. This suggests that the temperature fluctuation is mainly created by the eddy motion. The stress $\overline{V'U'}$ is maximum at the center of the cavity.

Results of direct numerical simulations for $Gr = 1 \times 10^9$ ($Pr = 0.022$) are presented in Fig. 5, which shows the plot of temporal variation of V-velocity at the center of the cavity with the corresponding power spectra. The time-averaged temperature profiles compare very well with the predictions of the two-dimensional LRN k–ε turbulence model (Fig. 6(a)). The results also confirm the formation of a thin shear layer near the horizontal boundaries (Fig. 6(b)). Peak-to-peak temperature variation at the center of the cavity is very significant (about 40% of the applied temperature difference along the boundaries), and this is revealed in Fig. 7(a). The Reynolds stresses $\overline{V'\theta'}$ and $\overline{V'U'}$ are shown in Fig. 7(b). The $-\overline{V'U'}$ stress term has a maximum at the center of the cavity, but $\overline{V'\theta'}$ has two maxima at the horizontal boundaries which decrease to a minimum at the core of the cavity. The power spectra suggest that the flow is dominated by the large eddies associated with small eddies.

Differentially heated cavity

Experiments on differentially heated cavities and at high Rayleigh numbers filled with liquid metals are very limited. Most studies have been done in the laminar or the transition regimes. Viskanta *et al.* [6] reported experimental data for temperature profiles in a cavity filled with gallium ($Pr = 0.0208$) for $Ra = 1.08 \times 10^6$. Also, Wolf *et al.* [7] measured temperature profiles in a cavity filled with liquid tin ($Pr = 0.011$) for $Ra = 3.66 \times 10^5$. Their results show that the flow is fluctuating, but no further analysis was carried out to identify if the flow was fully turbulent. However, a two-dimensional LRN k–ε turbulence model was used to simulate natural convection flow and heat transfer in a differentially heated cavity having an aspect ratio of one and filled with a liquid. A nonuniform mesh grid of 61×61 was used and

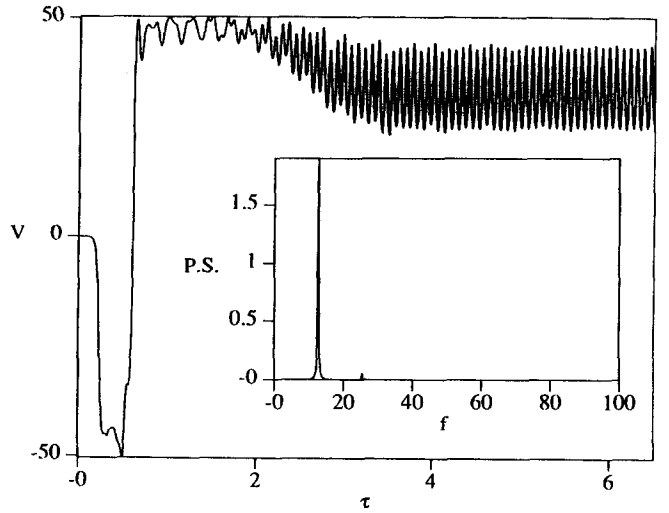

FIG. 2. V-velocity variation with time and corresponding power spectra for a cavity heated from below for $Ra = 2.2 \times 10^5$ and $Pr = 0.022$.

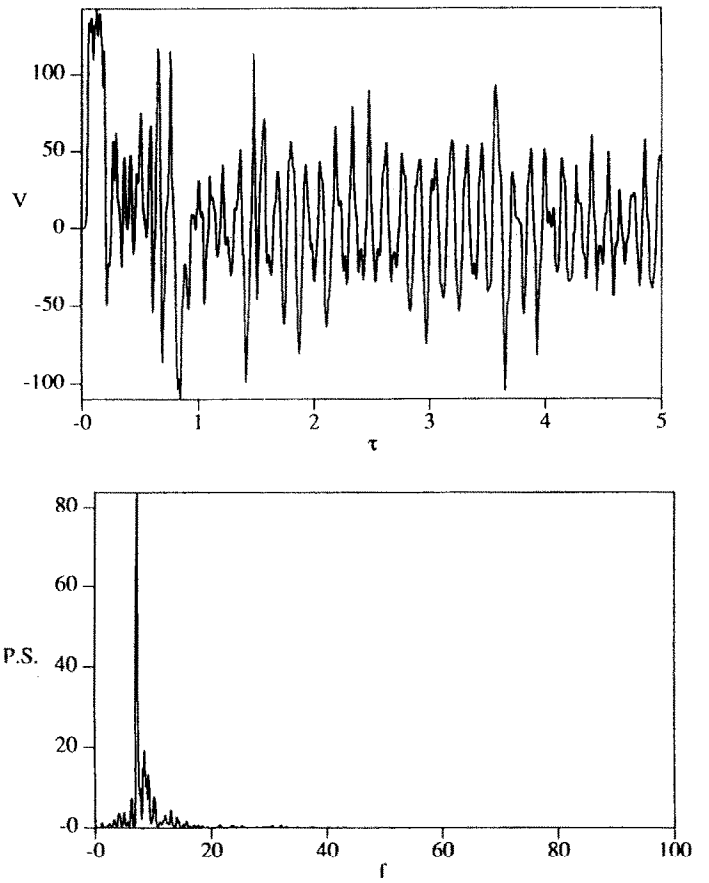

FIG. 3. V-velocity variation with time and corresponding power spectra for a cavity heated from below for $Ra = 2.2 \times 10^6$ and $Pr = 0.022$.

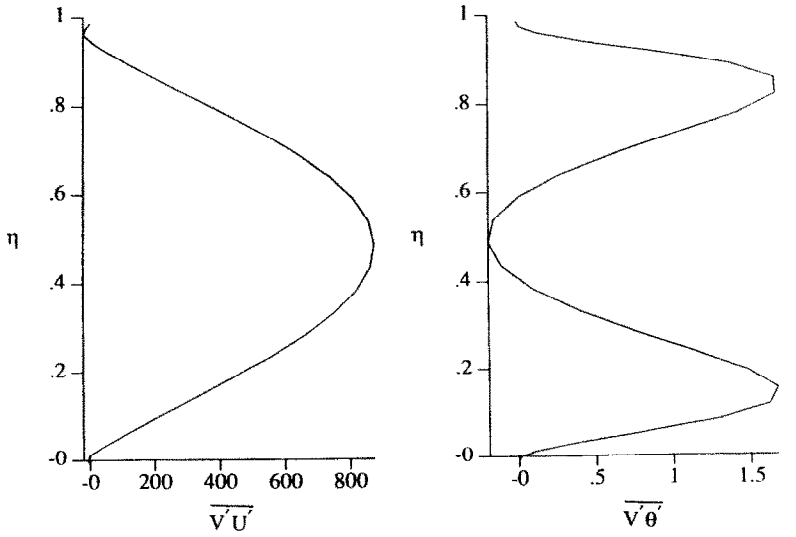

FIG. 4. Reynolds stress correlation profiles for cavity heated from below, $Ra = 2.2 \times 10^6$ and $Pr = 0.022$.

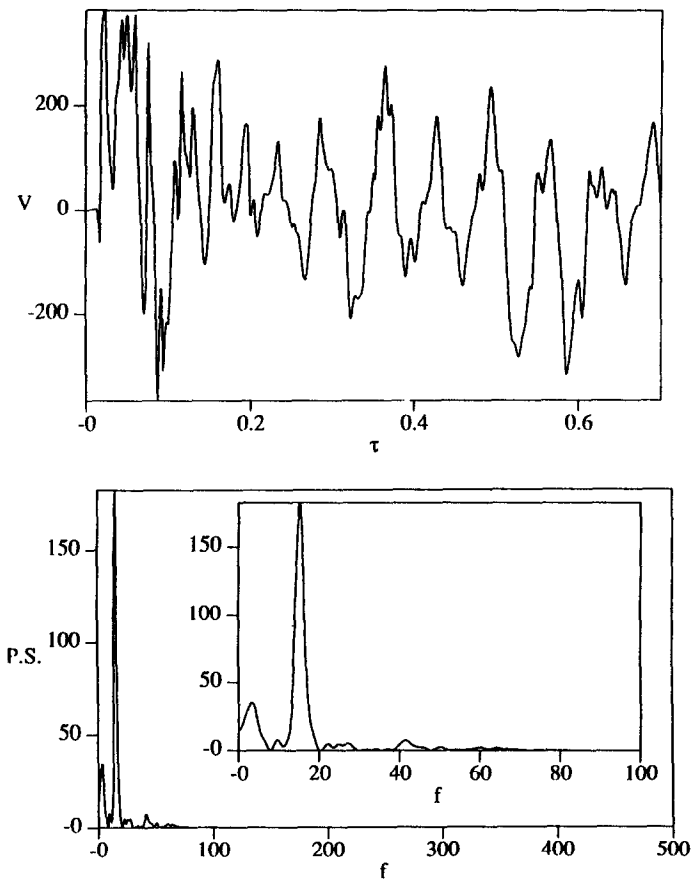

FIG. 5. V-velocity variation with time and corresponding power spectra for a cavity heated from below for $Ra = 2.2 \times 10^7$ and $Pr = 0.022$.

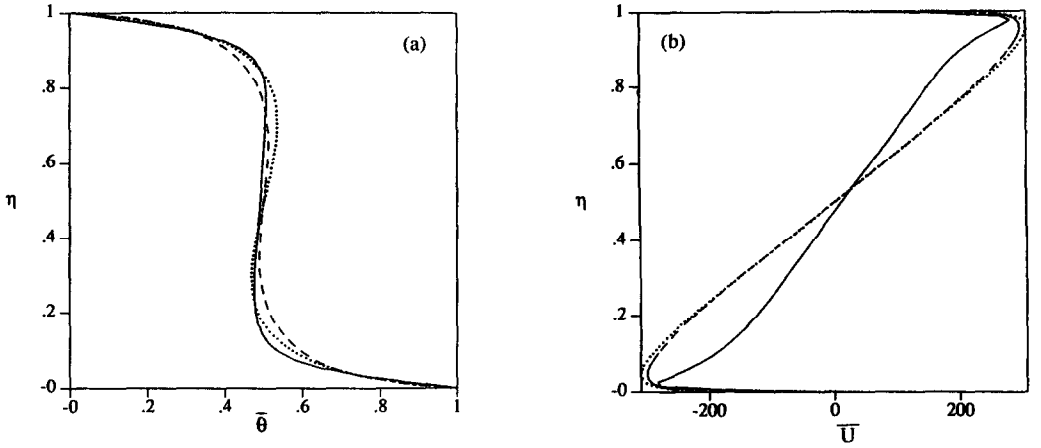

FIG. 6. Temperature profiles at the center of the cavity predicted by different models (a) and U-velocity profile at the center of the cavity (b) predicted by different models for $Pr = 0.022$ and $Ra = 2.2 \times 10^7$; ——, 3-D unsteady; – – –, 2-D k–ε model, $Pr_t = 1.2$; · · · · ·, 2-D k–ε model, $Pr_t = 1.4$.

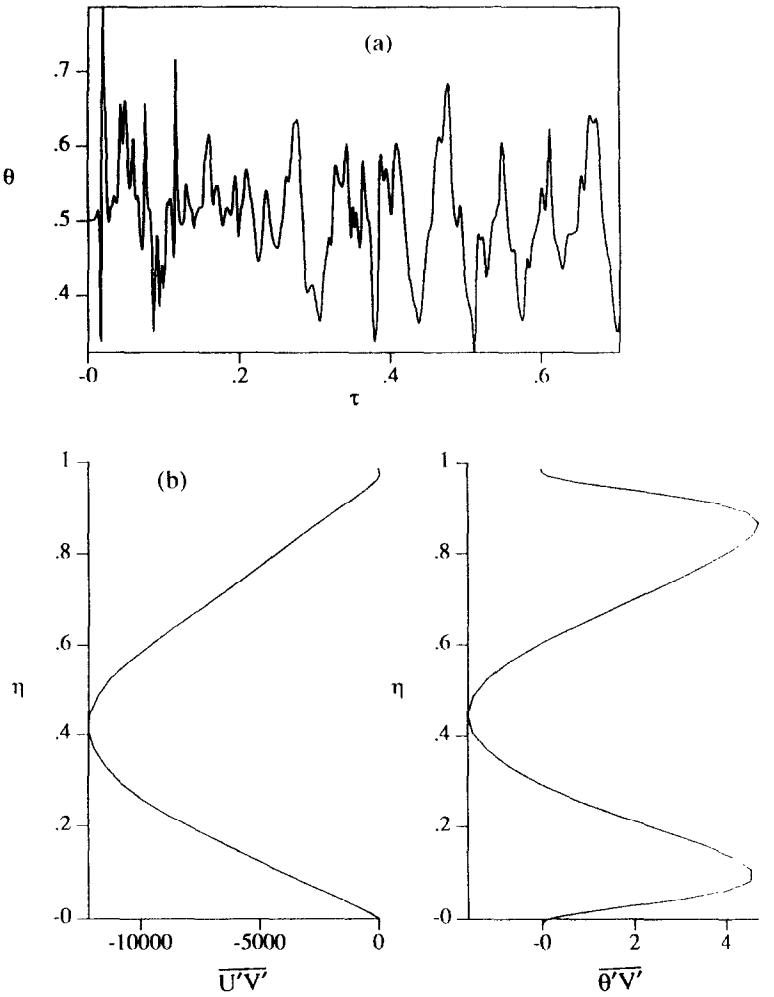

FIG. 7. Variation of temperature with time at the center of the cavity (a) and Reynolds stress components (b) for cavity heated from below with $Ra = 2.2 \times 10^7$ and $Pr = 0.022$.

$Pr_t = 1.2$ was employed. A comparison of the results of the simulation with the experimental data is given in Fig. 8 and shows good agreement. The flow structure for $Pr = 0.011$ and $Ra = 3.66 \times 10^5$ reveals weak secondary circulations at the corners of the cavity, in addition to the main circulation [7]. For $Ra = 1.08 \times 10^6$ and $Pr = 0.0208$, the flow structure contains secondary circulations inside the main circulation.

A direct numerical simulation was carried out for a cubic cavity of $1 \times 1 \times 1$ in ξ-, η- and ζ-directions with $Gr = 1 \times 10^9$ and $Pr = 0.022$. A dimensionless time step of 0.005 was used and a $31 \times 31 \times 31$ non-uniform mesh was employed. The temporal variation of the Nusselt number at the vertical walls is shown in Fig. 9. The results indicate that the transient period is very short ($\tau < 0.2$), and the flow fluctuates around an average Nusselt number of 13.68.

The results of the 2-D and 3-D LRN k–ε turbulence models using $Pr_t = 1.2$ are compared with direct numerical simulations (Fig. 10). It is clear that the agreement between the three model predictions is consistent. Inspecting the flow field showed that the flow is two-dimensional except near the boundaries. The flow structure consists of three secondary circulations inside the main circulation (Fig. 11). Increasing the Rayleigh number increases the complexity of the flow, and this is evident from Fig. 11. A similar conclusion can be drawn for $Pr = 0.005$, where the flow structure showed a similar pattern at the same Bo.

The spatial and temporal average Nusselt number for the Rayleigh number range between 5×10^3 and 2.2×10^7 and the Prandtl number range from 0.022 to 0.005 investigated can be best-fit to the correlation (Fig. 12) of the form

$$\overline{Nu}_{av} = 0.386 Bo^{0.286}. \tag{11}$$

The above correlation is for heat transfer in a cavity having an aspect ratio of unity. Extensive calculations were carried out for cavities having aspect ratios of 1/2, 1/4 and 1/6 using mesh sizes ranging from 81×41 to 151×41. Accordingly, the above correlation can be modified as

$$\overline{Nu}_{av} = 0.386 Bo^{0.286} A^{0.213} \tag{12}$$

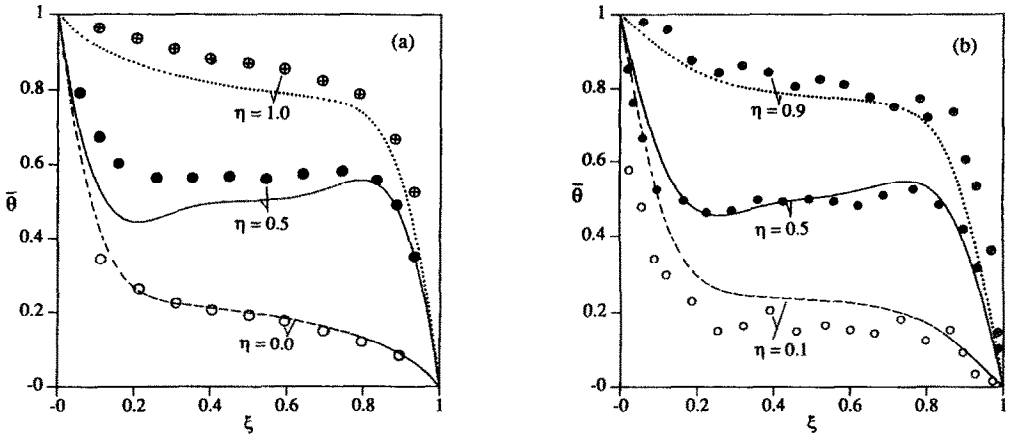

FIG. 8. (a) Comparison of experimental data [6] with predictions for a differentially heated cavity with $Ra = 1.08 \times 10^6$ and $Pr = 0.0208$. (b) Comparison of experimental data [7] with predictions for a differentially heated cavity with $Ra = 3.66 \times 10^5$ and $Pr = 0.011$.

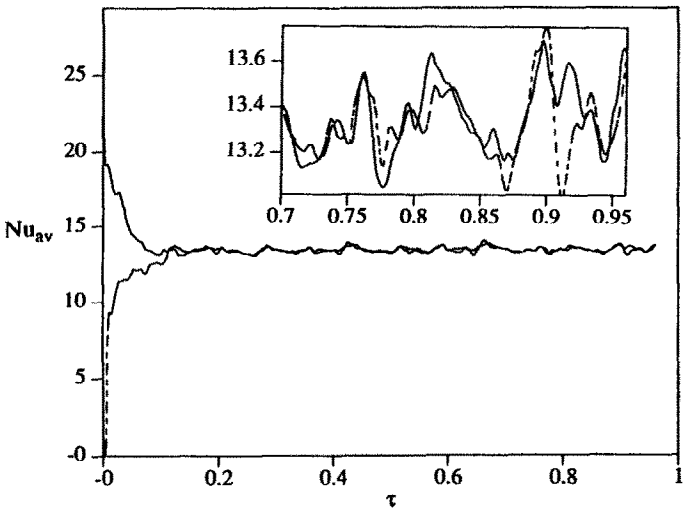

FIG. 9. Temporal variation of Nusselt number at the vertical walls for $Ra = 2.2 \times 10^7$ and $Pr = 0.022$: solid line is for the heated wall and the dashed line is for the cold wall.

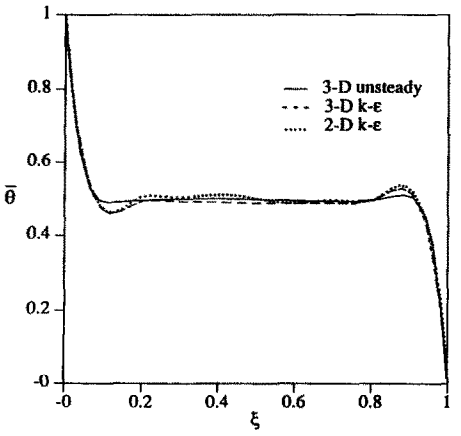

FIG. 10. Comparison of temperature profiles at the mid-height of the differentially heated cavity for $Ra = 2.2 \times 10^7$ and $Pr = 0.022$.

to account for the aspect ratio. Laminar natural convection flow and heat transfer in a cubic cavity has been investigated [6, 8, 9]. Mohamad and Viskanta [8, 9] used a very fine mesh and second-order accurate numerical scheme in their numerical calculations. Their predicted average Nusselt numbers for the range of Prandtl number investigated (0.01–0.005) can be fit by the following correlation:

$$\overline{Nu_{av}} = 1.05 Bo^{0.168}. \tag{13}$$

This correlation is plotted in Fig. 12 and intersects the correlation (equation (11)) for turbulent flow results at $Bo = 4.8 \times 10^3$. Hence, it is assumed that the flow in a cubic cavity heated from a side becomes turbulent for $Bo > 4.8 \times 10^3$ for low Prandtl number fluids.

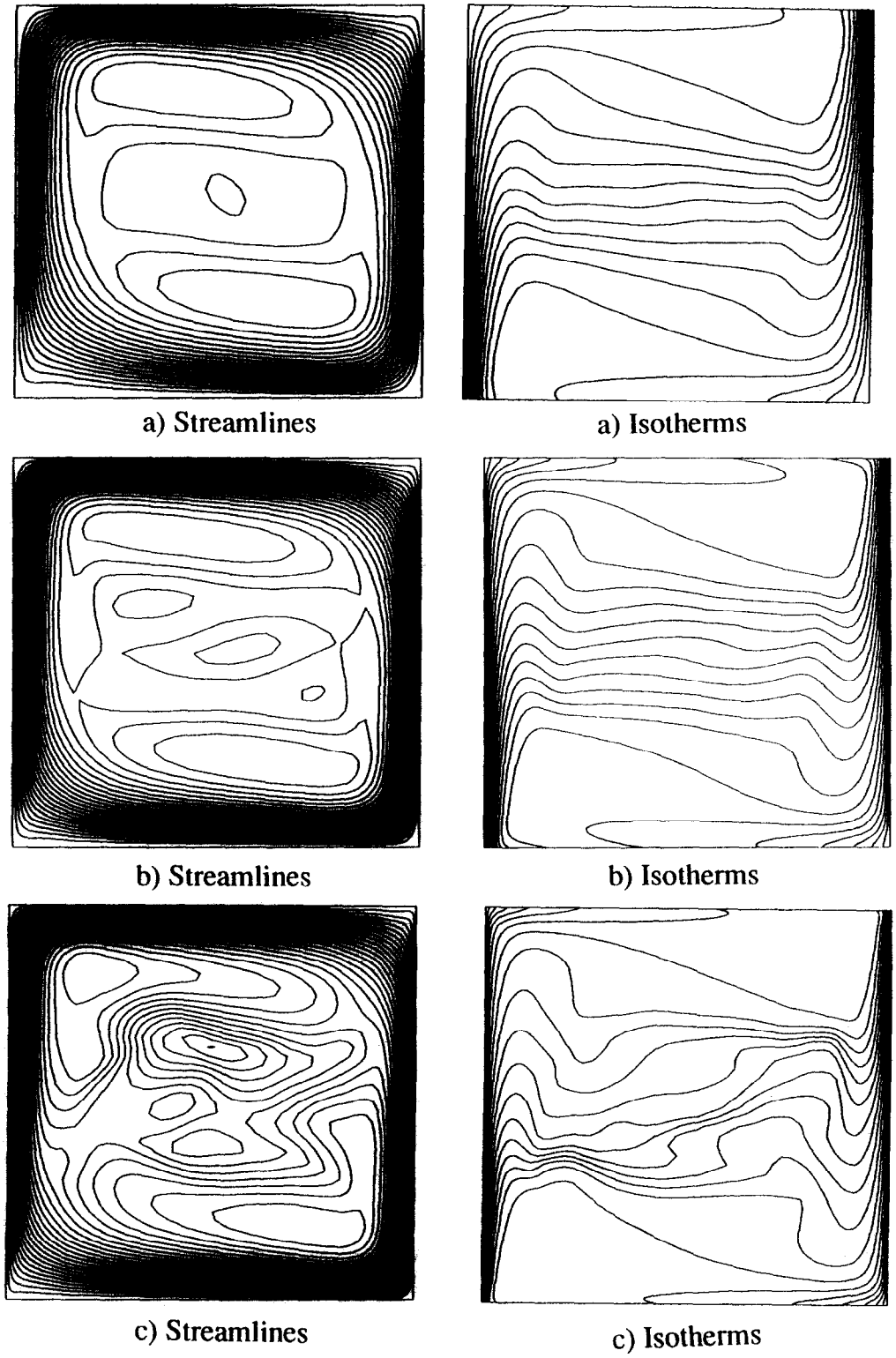

FIG. 11. Streamlines and isotherms for differentially heated cavity for $Pr = 0.022$: (a) $Ra = 2.2 \times 10^7$, (b) $Ra = 2.2 \times 10^8$ and (c) $Ra = 2.2 \times 10^9$.

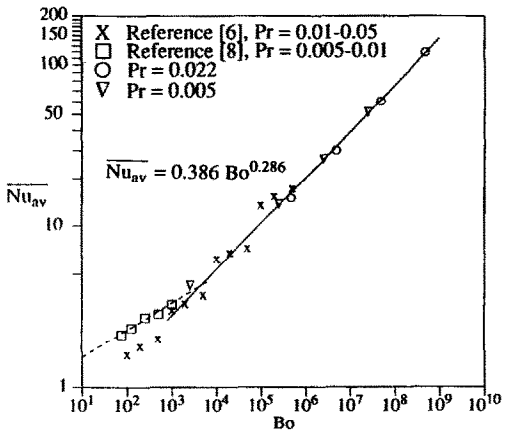

FIG. 12. Nusselt number correlations for a differentially heated cavity.

CONCLUSIONS

Turbulent natural convection flow in cavities heated from below and cooled from above or heated differentially and filled with low Prandtl number fluids are investigated. Direct numerical simulations and two- and three-dimensional LRN k–ε turbulence model predictions are compared with available experimental data. Results revealed that using turbulent Prandtl number of one or slightly greater than one in the k–ε turbulence model can produce useful results regardless of the molecular Prandtl number. These results are supported by direct numerical simulations and by available experimental data.

Buoyant flows in cavities heated from below are three-dimensional in nature, but the heat transfer predicted by the two-dimensional LRN k–ε turbulence model are comparable with the available experimental data. The flow is periodic for $Ra = 2.2 \times 10^5$ with $Pr = 0.022$ for a cavity heated from below and becomes aperiodic for $Ra \geqslant 2.2 \times 10^6$. Very thin shear layers are evident at the horizontal boundaries of the cavity heated from below.

The flow in a differentially heated cavity is two-dimensional, except very near the boundaries, where evidence of three-dimensionality is weak. Heat transfer results can be correlated as a function of Bo ($= Ra\ Pr$). Hence, a correlation was suggested for turbulent flow in a differentially heated cavity of aspect ranges from 1 to 1/6 and for the range of the parameter investigated ($Ra \geqslant 5 \times 10^3$ and $Pr = 0.022$–0.005)

$$\overline{Nu_{av}} = 0.386 Bo^{0.286} A^{0.213}. \quad (14)$$

Also, the results of Mohamad and Viskanta [8] are correlated for laminar flow. The intercept of the two correlations suggests that the buoyant flow in differentially heated cavities of aspect ratio of unity become turbulent for $Bo > 4.8 \times 10^3$.

REFERENCES

1. D. V. Julian and R. G. Akin, Experimental investigation of natural convection heat transfer to mercury, *I & EC Fundam.* **8**, 641–646 (1969).
2. D. D. Papailiou and P. S. Lykoudis, Turbulent free convection flow, *Int. J. Heat Mass Transfer* **17**, 161–172 (1974).
3. W. W. Humphrey and J. R. Welty, Natural convection with mercury in a uniformly heated vertical channel during unstable laminar and transitional flow, *Am. Ind. Chem. Engng J.* **21**, 268–274 (1975).
4. N. Sheriff and N. W. Davies, Liquid metal natural convection from plane surface: a review including recent sodium measurements, *Int. J. Heat Fluid Flow* **1**, 149–154 (1979).
5. M. Uotani, Natural convection heat transfer in thermally stratified liquid metal, *J. Nucl. Sci. Technol.* **24**, 442–451 (1987).
6. R. Viskanta, D. M. Kim and C. Gau, Three-dimensional natural convection heat transfer of a liquid metal in a cavity, *Int. J. Heat Mass Transfer* **29**, 475–485 (1986).
7. F. Wolff, C. Beckermann and R. Viskanta, Natural convection of liquid metals in vertical cavities, *Exp. Thermal Fluid Sci.* **1**, 83–91 (1988).
8. A. A. Mohamad and R. Viskanta, Transient natural convection of low Prandtl number fluids in a differentially heated cavity, *Int. J. Numer. Meth. Fluids* **13**, 61–81 (1991).
9. A. A. Mohamad and R. Viskanta, Transient low Prandtl number fluid convection in a lid-driven cavity, *Numer. Heat Transfer* **19**, 187–205 (1991).
10. A. A. Mohamad and R. Viskanta, Transition to chaos in a differentially heated square cavity filled with a liquid metal. In *Advanced Computational Methods in Heat Transfer, Vol. 2: Natural and Forced Convection, Proc. First Int. Conf.* (Edited by L. C. Wrobel, C. A. Brebbia and A. J. Nowak), pp. 159–169. Computational Mechanics Publications, Southampton (1990).
11. I. Celik, T. Kobayshi, K. N. Ghia and J. Kurokawar, Editors, *Advances in Numerical Simulation of Turbulent Flows (Proc. First ASME/JSME Fluid Engineering Conf.*, Portland, Oregon, 23–27 June 1991). ASME, New York (1991).
12. J. A. C. Humphrey, F. S. Sherman and W. M. To, Numerical simulation of buoyant turbulent flow, Sandia National Laboratories, Report 85-8180 (1985).
13. C. J. Lawn, Turbulent temperature fluctuations in liquid metals, *Int. J. Heat Mass Transfer* **20**, 1035–1044 (1977).
14. A. J. Reynolds, *Turbulent Flows in Engineering*. Wiley, New York (1974).
15. N. Z. Ince and B. E. Launder, On the computation of buoyancy-driven turbulent flows in rectangular enclosures, *Int. J. Heat Fluid Flow* **12**, 110–117 (1989).
16. A. J. Reynolds, The prediction of turbulent Prandtl and Schmidt numbers, *Int. J. Heat Mass Transfer* **18**, 1055–1069 (1975).
17. H. O. Buhr, A. D. Carr and R. E. Balzhiser, Temperature profiles in liquid metals and the effect of superimposed free convection in turbulent flow, *Int. J. Heat Mass Transfer* **11**, 641–654 (1968).
18. N. Z. Azer and B. T. Chao, A mechanism of turbulent heat transfer in liquid metals, *Int. J. Heat Mass Transfer* **1**, 121–138 (1960).
19. P. S. Lykoudis and Y. S. Touloukian, Heat transfer in liquid metals, *Trans. ASME* **80**, 653–667 (1958).
20. R. G. Deissler, Turbulent heat transfer and temperature fluctuations in a field with uniform velocity and temperature gradients, *Int. J. Heat Mass Transfer* **6**, 257–270 (1963).
21. M. A. Cotton, J. D. Jackson and L. S. L. Yu, Application of a low-Reynolds-number two-equation turbulence model to mercury and sodium flows in the turbulent mixed convection regime. In *Seventh Symposium on Tur-*

bulent Shear Flows, Stanford University, 21–23 August, pp. 20.5.1–20.5.6 (1989).
22. S. Aoki, A consideration on the heat transfer in liquid metal, *Bull. Tokyo Inst. Technol.* **54**, 63–73 (1968).
23. M. Jischa and H. B. Rieke, Turbulent heat transfer. In *Recent Contributions to Fluid Mech.* (Edited by W. Hasse). Springer, New York (1983).
24. E. Yu. Krasil'nikov, The effect of a transverse field on convective heat transfer in a conductive-fluid duct flow. In *Magnetohydrodynamic Flow in Ducts* (Edited by H. Branover). Wiley, New York (1978).
25. A. S. Monin and A. M. Yaglom, *Statistical Fluid Mechanics: Mechanics of Turbulence*, Vol. 1. MIT Press, Cambridge, MA (1965).
26. V. F. Potemkin, Universal profiles and law of turbulent near-wall heat and mass transfer, *J. Engng Phys.* **55**, 545–553 (1988).
27. V. V. Golubev, Approximate solution of a problem of convective heat transfer between a plate and liquid metals, *J. Engng Phys.* **57**, 253–258 (1990).
28. R. A. Antonia and J. Kim, Turbulent Prandtl number in the near-wall region of a turbulent channel flow, *Int. J. Heat Mass Transfer* **34**, 1905–1908 (1991).
29. K. Bremhorst and L. Krebs, Experimentally determined turbulent Prandtl numbers in liquid sodium at low Reynolds numbers, *Int. J. Heat Mass Transfer* **35**, 351–359 (1992).
30. R. B. Brid, W. E. Stewart and E. Lightfoot, *Transport Phenomena*. Wiley, New York (1960).
31. A. A. Mohamad and R. Viskanta, Application of low Reynolds number k–ε turbulence model to buoyant and mixed flows in a cavity. In *Fundamentals of Mixed Convection* (Edited by T. S. Chen and T. Y. Chu), pp. 43–54. ASME, New York (1992).
32. S. V. Patankar, *Numerical Heat Transfer and Fluid Flow*. Hemisphere, New York (1980).
33. P. J. Roache, *Computational Fluid Dynamics*. Hermosa, Albuquerque, New Mexico (1976).
34. G. Ahlers and R. P. Behringer, The Rayleigh–Bénard instability and the evolution of turbulence. In *Supplement of the Progress of Theoretical Physics*, No. 64, pp. 186–201. Physical Society of Japan, Tokyo (1978).
35. S. Globe and D. Dropkin, Natural convection heat transfer in liquids confined between two horizontal plates, *J. Heat Transfer* **81**, 24–29 (1959).
36. H. T. Rossby, A study of Bénard convection with and without rotation, *J. Fluid Mech.* **36**, 309–335 (1969).
37. S. Fauve, Competing instability in Rayleigh–Bénard convection. In *Current Trends in Turbulent Research, Progress in Astronautics and Aeronautics* (Edited by H. Branover, M. Mond and Y. Unger), pp. 65–77. AIAA, Washington, DC (1988).
38. A. A. Mohamad, Mixed convection in lid-driven shallow cavities, Ph.D. Thesis, Purdue University, West Lafayette, Indiana (1992).
39. J. W. Deardorff and G. E. Willis, The effect of two-dimensionality on the suppression of thermal turbulence, *J. Fluid Mech.* **23**, 337–353 (1965).